UCRL- 92446
PREPRINT

DIELECTRONIC RECOMBINATION RATE COEFFICIENTS FOR NEON-LIKE IONS

Sam Dalhed
Joseph Nilsen
Peter Hagelstein

THIS PAPER WAS PREPARED FOR SUBMITTAL TO
Physical Review A

April 4, 1985

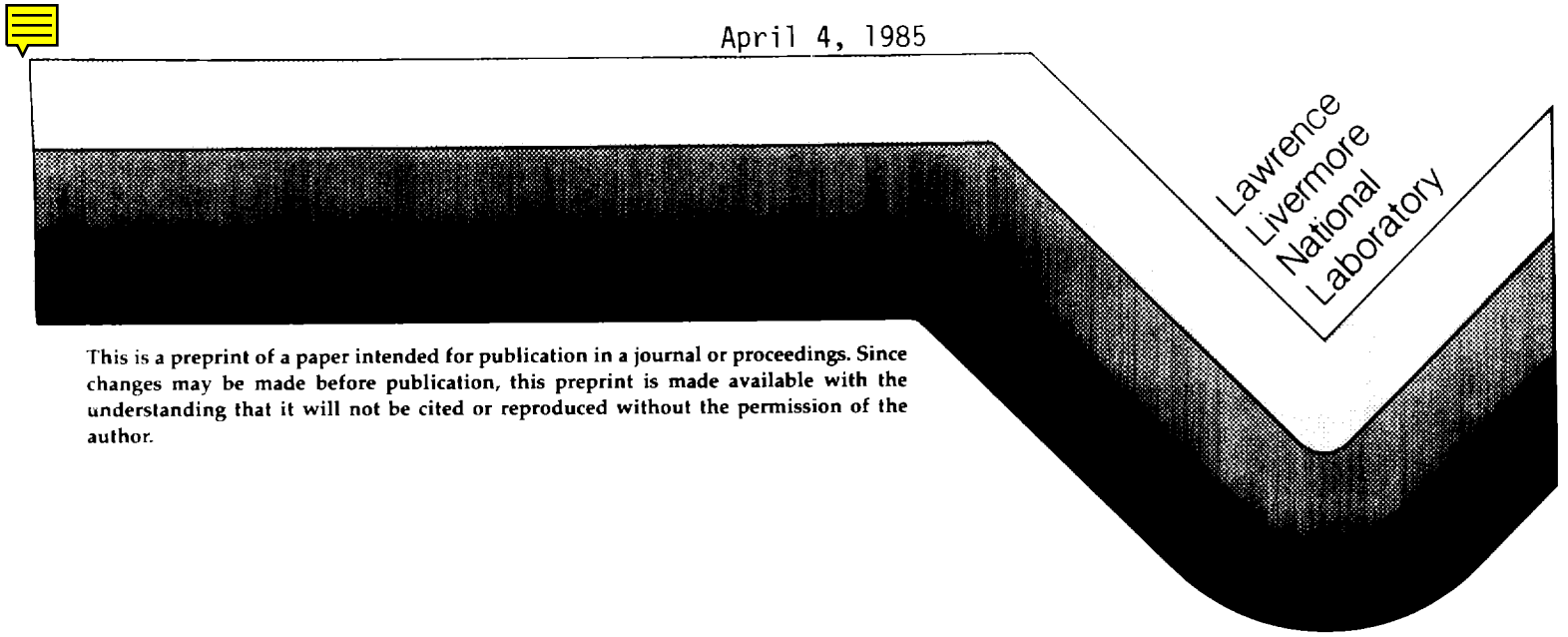

Dielectronic recombination rate coefficients for neon-like ions[†]

Sam Dalhed, Joseph Nilsen, and Peter Hagelstein

Lawrence Livermore National Laboratory
Livermore, California 94550

ABSTRACT

This paper presents for the first time an explicit calculation of the dielectronic rate coefficients for seventeen neon-like ions ranging from argon to tungsten using relativistic multi-configuration wavefunctions to calculate both the Auger and radiative matrix elements. The effect of electron collisions on the dielectronic rate coefficient is also examined at several densities of interest for modeling laboratory plasmas.

April 3, 1985

[†]Work performed under the auspices of the U. S. Department of Energy by the Lawrence Livermore National Laboratory under contract No. W-7405-ENG-48.

Dielectronic recombination rate coefficients for neon-like ions[†]

Sam Dalhed, Joseph Nilsen, and Peter Hagelstein

Lawrence Livermore National Laboratory
Livermore, California 94550

1. Introduction

Dielectronic recombination is the dominant recombination process for ions in high temperature low density plasmas[1] such as the solar corona. It is also a significant contributor to plasma cooling in hot plasmas found in laboratory fusion plasma experiments[2]. The calculation of the dielectronic rate coefficient α^{DR} is difficult because of the many intermediate resonance states over which the rate needs to be summed . We calculate α^{DR} for recombination from the neon-like ground state into the sodium-like non-autoionizing states via the 3l3l' manifold for seventeen neon-like ions ranging from Ar^{+8} to W^{+64}. This calculation uses accurate relativistic atomic wavefunctions calculated for each ion. This is the first calculation in which relativistic multi-configuration wavefunctions are used to calculate the matrix elements explicitly for each of the doubly excited states. Previous authors have calculated α^{DR} using a simple angular momentum averaged procedure[3] to average over as many intermediate states as possible or have done a detailed calculation using single or few configuration non-relativistic wave functions to calculate the relevant atomic data[4-6].

2. Method

In j-j coupling the 3l3l' manifold consists of 237 doubly excited states which are connected to the neon-like ground state $1s^2 2s^2 2p^6$ by the Auger process and to the five sodium-like non-autoionizing states $[KL]3s_{1/2}, 3p_{1/2}, 3p_{3/2}, 3d_{3/2}, 3d_{5/2}$

by radiative decay and electron collisional de-excitation. In addition the doubly excited states are connected to each other by radiative decay and electron collisional processes.

There are a total of 243 states in our model. Our first task was to calculate the wavefunctions for each of these states using the code YODA, which we ran on a CDC7600 computer. YODA is a relativistic multi-configuration Hartree-Fock atomic physics code which uses as its orbital basis a set of single configuration Dirac orbitals calculated in a spherically symmetric central potential which includes a finite nuclear potential. Racah algebra is used in calculating the angular momentum part of the matrix elements. Using these fixed orbitals to construct the single configuration wavefunctions, the Hamiltonian matrix is calculated including Breit corrections to the Coulomb interactions between the electrons. Also included are the quantum electrodynamic effects such as self energy[7] and vacuum polarization[8]. The Hamiltonian is diagonalized to give the full multi-configuration wavefunctions in intermediate coupling. These wavefunctions are then used to calculate the oscillator strengths for all the dipole allowed transitions.

The continuum orbitals used in computing the Auger matrix elements were calculated in a distorted wave approximation neglecting exchange. The potential was a spherically averaged final state potential. For this work, an ion in a neon-like ground state would be used to calculate the potential. For the high Z systems we are using, the neglect of the exchange term should be a small effect. The free electron wavefunctions are used with the multi-configuration wavefunctions for the bound electrons to calculate the Auger matrix elements.

Approximate collision cross sections are computed in the classical path approximation[9] coupling dipole allowed states. These collision cross sections are then approximated by the five parameter fit

$$< \sigma\, v > \; = 1.58 \; X \; 10^{-5} \; p(b) \; \frac{e^{-b}}{(b \; \theta^{3/2})} \; \frac{cm^3}{sec} \qquad (1)$$

where

$$b = \frac{\delta E}{\theta} \qquad (2)$$

and

$$ln(p(b)) = a0 + a1 \; ln(b) + a2 \; \ln^2(b) + a3 \; \ln^3(b) \; . \qquad (3)$$

δE is the transition energy(in eV) used in fitting the data and θ=kT is the electron temperature(in eV). The free electrons of density n_e are assumed to have a Maxwell Boltzmann velocity distribution represented by a temperature T.

The components of the dielectronic recombination process are:

Dielectronic capture, Auger: $X^{+z} + e \rightarrow X^{+(z-1)} \; (\overline{2l_1} \; 3l_2 \; 3l_3)$

Stabilization: $X^{+(z-1)} \; (\overline{2l_1} \; 3l_2 \; 3l_3) \rightarrow X^{+(z-1)}(3l_3) + h\nu$

The neon-like ground state X^{+z} captures an electron to form a doubly excited sodium-like state $X^{+(z-1)}(\overline{2}l3l3l')$. The notation $\overline{2}l$ represents a hole in the neon-like core while 3l3l' represents the two n=3 electrons. The doubly excited state can Auger decay or undergo a radiative decay($\Delta n = 1$) to a sodium-like non-autoionizing state which stabilizes the capture process.

In addition to the "direct" dielectronic recombination there are radiative processes and (for finite density plasmas) collisional processes which can cause angular momentum redistribution within the doubly excited states and collisional de-excitation to the sodium-like non-autoionizing states which stabilize the capture. These processes are shown below:

Radiative decay processes: $X^{+(z-1)}(\overline{2l_1} \; 3l_2 \; 3l_3) \rightarrow X^{+(z-1)}(\overline{2l_1} \; 3l_2' \; 3l_3) + h\nu$

$X^{+(z-1)}(\overline{2l_1} \; 3l_2 \; 3l_3) \rightarrow X^{+(z-1)}(\overline{2l_1'} \; 3l_2 \; 3l_3) + h\nu$

Collisional Excitation and *De−excitation*: $X^{+(z-1)}(\overline{2l_1}\ 3l_2\ 3l_3) + e \rightarrow X^{+(z-1)}(3l_3) + e$

$$X^{+(z-1)}(\overline{2l_1}\ 3l_2\ 3l_3) + e \rightarrow X^{+(z-1)}(\overline{2l_1}\ 3l_2'\ 3l_3) + e$$

$$X^{+(z-1)}(\overline{2l_1}\ 3l_2\ 3l_3) + e \rightarrow X^{+(z-1)}(\overline{2l_1'}\ 3l_2\ 3l_3) + e$$

All of the above processes are included in our calculation.

To calculate the population kinetics, let

N_I = population of the neon-like ground state

N_j = population of the doubly excited states j = 1 to 237

N_{F_i} = population of the sodium-like non-autoionizing states i = 1 to 5

R_{ab} = rate coefficient for transitions from level a to level b

then

$$\frac{dN_I}{dt} = \sum_k N_k\ R_{kI} - N_I \sum_k R_{Ik} \tag{4}$$

$$\frac{dN_j}{dt} = N_I\ R_{Ij} - N_j\ [R_{jI} + R_{jF_i} + \sum_k R_{jk}] + \sum_k N_k\ R_{kj} \tag{5}$$

$$\frac{dN_{F_i}}{dt} = \sum_k N_k\ R_{kF_i} \tag{6}$$

We then calculate the populations of the doubly excited states using dynamic relaxation to steady state. We assume the population of the neon-like ground state is constant N_I and that the populations of the sodium-like non-autoionizing states are zero. Equation 5 is solved for N_j by setting $dN_j/dt = 0$ and then iterating on

$$N_j = \frac{N_I\gamma_j^{DI} + \sum_k N_k\ R_{kj}}{\gamma_j^A + \gamma_j^R + \gamma_j^C + \sum_k R_{jk}} \tag{7}$$

where $\gamma_j^{DI} = R_{Ij}$ is the dielectronic capture rate which is calculated by detailed balance from the Auger rate γ_j^A.

$$\gamma_j^{DI}(\theta) = \frac{h^3\, n_e}{(2\pi m\theta)^{3/2}} \frac{g_j \gamma_j^A}{2g_I} e^{\frac{-\Delta E_j}{\theta}} \tag{8}$$

where

g_j = degeneracy of the doubly excited state j

g_I = degeneracy of the neon-like ground state

E_j = energy of the doubly excited state j

E_I = energy of the neon-like ground state

$\Delta E_j = E_j - E_I$

The radiative decay rate γ_j^R and the collisional de-excitation rate γ_j^C stabilize dielectronic capture by the $\Delta n = 1$ transitions.

$$\gamma_j^R + \gamma_j^C = \sum_{i=1}^{5} R_{jFi} \tag{9}$$

We define the total destruction rate γ_j^D to be

$$\gamma_j^D = \gamma_j^R + \gamma_j^C + \sum_k R_{jk} \tag{10}$$

where the last term is due to $\Delta n = 0$ transitions. The recombination rate is then calculated by summing the flux of population from the doubly excited states to the sodium-like non-autoionizing states.

$$\gamma^{DR} = \sum_{j=1}^{237} N_j \left[\gamma_j^R + \gamma_j^C\right] \tag{11}$$

The dielectronic recombination rate coefficient α^{DR} is defined by

$$\alpha^{DR} = \frac{\gamma^{DR}}{n_e\, N_I} \tag{12}$$

The inclusion of the radiative decay rates for the $\Delta n = 0$ transitions increases the rate coefficient by less than 3% for the range of ions we considered.

3. Results

We calculated the dielectronic rate coefficient α^{DR} for the neon-like isoelectronic sequence as a function of electron temperature for each of the seventeen elements Ar, Fe, Cu, Ge, Kr, Zr, Nb, Mo, Ru, Rh, Ag, Sn, Xe, Nd, Ho, Ta, and W at an electron density $n_e = 10^{14} / cc$. At this density, the effect of electron collisions is negligible and can be neglected as we will show later. In figure 1 we plot α^{DR} versus θ for six of the elements. In table I we list the maximum value of the dielectronic rate coefficient α^{DR}_{MAX} for each element and the value of θ_0 at which α^{DR} is maximum. Also listed is $\bar{E}$, the average energy lost by an electron in each recombination. $\bar{E}$ is calculated by

$$\bar{E} = \frac{\sum_j \Delta E_j \omega_j}{\sum_j \omega_j} \tag{13}$$

where

$$\omega_j = \frac{\gamma_j^{DI} \gamma_j^R}{\gamma_j^R + \gamma_j^A} \tag{14}$$

We calculate ω_j at θ_0. The $\sum_j \omega_j$ is a fast numerical algorithm[10] to calculate an approximate γ^{DR}. If we model dielectronic recombination via the 3l3l' manifold as proceeding through one pseudo doubly excited state with $\Delta E = \bar{E}$ then we may fit the relativistic multi-configuration rate coefficient by

$$\alpha^{DR} = \frac{4.4817\ \alpha^{DR}_{MAX}\ e^{-\frac{3}{2x}}}{x^{\frac{3}{2}}} \qquad x = \frac{3\theta}{2\bar{E}} \tag{15}$$

where α^{DR} is maximum at $\theta = \frac{2}{3}\bar{E}$. (Comparing $\bar{E}$ and θ_0 in table I, we see that $\theta_0 \approx \frac{2}{3}\bar{E}$ within 1% for all elements). Figure 2 shows α^{DR} plotted versus θ for Nb demonstrating excellent agreement between the fit and the original data.

The open circles are a result of the detailed calculation while the solid line represents the fit of equation 15. Agreement is better that 1% over the range of $.5 < x < 5$. In general, this fit is good to 4% over the same range of x for all the ions calculated. At low temperatures, the fit underestimates α^{DR} because the detailed system has lower energy states which become more heavily weighted, therefore $\bar{E}$ is no longer the appropriate energy to use for the pseudo state.

Figure 3 plots α^{DR}_{MAX} versus Z(the bare nuclear charge) for this calculation(open circles) and the Burgess-Merts[2,11] formula(solid line). We note that our calculation for the dielectronic recombination rate peaks at Niobium($Z = 41$) while the Burgess-Merts formula peaks at Al. The Burgess-Merts formula used is

$$\alpha^{DR} = 2.395 \; X \; 10^{-9} \; \frac{B(z)}{\theta^{3/2}(ineV)} \bar{f}_{lj} \; A(x) \; e^{\frac{-\Delta E_j}{\theta}} \; \frac{cm^3}{sec} \tag{16}$$

with $z = Z - 10 =$ charge number of the recombining ion and

$$B(z) = \frac{z^{1/2}(z+1)^{5/2}}{(z^2 + 13.4)^{1/2}} \tag{17}$$

$$A(x) = \frac{.5 \; x^{1/2}}{1 + .210x + .030x^2} \tag{18}$$

$$\Delta E_j = \frac{13.606}{a}(z+1)^2\left(\frac{1}{n_f^2} - \frac{1}{n_j^2}\right) \tag{19}$$

$$a = 1 + \frac{.015z^3}{(z+1)^2} \tag{20}$$

$$x = (z+1)\left(\frac{1}{n_f^2} - \frac{1}{n_j^2}\right) \tag{21}$$

with $\bar{f}_{lj}$ the average absorption oscillator strength for the 2l to 3l radiative stabilizing transition. We use $\bar{f} = .6412$, $n_l = 2$ and $n_j = 3$. We calculate ΔE_j and then use $\theta = 2\Delta E_j/3$ to calculate the maximum value of α^{DR} for the Burgess-Merts formula.

Collisions can have an effect on α^{DR} by redistributing the population of the doubly excited states among the different angular momentum states of the 3l3l' manifold, especially the higher angular momentum states. It can also act as a collisional stabilization process by collisionally de-exciting a 3l state to a 2l state. The latter process is very slow, however, except at very high electron densities. In figure 4 we plot $\alpha^{DR}(\theta=\theta_0)$ versus n_e for four neon-like ions spanning the range of Z we have considered. α^{DR} is normalized to unity for $n_e = 10^{14}$. As one might expect, the effect is largest for low Z.

To show the relative effects of angular momentum redistribution ($\Delta n = 0$) and collisional de-excitation($\Delta n = 1$) on the net dielectronic recombination rate coefficient we plot in figure 5 α^{DR} (at $\theta = \theta_0$) for argon versus electron density with(solid line) and without(dotted line) collisional de-excitation included in the calculation. Without collisional de-excitation α^{DR} reached a maximum around $n_e = 10^{21}$ and saturates. This saturation occurs when the collisional rates between the 3l3l' states dominates the Auger and radiative rates. The 3l3l' states are then in a thermal equilibrium with their relative populations determined by a Boltzmann distribution at the electron temperature. Any further increase in the collision rates($\Delta n = 0$) will not affect the population distribution since the states are already in local equilibrium. Also, heavy particle collisions[12] can contribute to the angular momentum redistribution especially at high temperatures for very small energy transitions.

As n_e continues to increase, collisional de-excitation($\Delta n = 1$) becomes dominant over radiative decay in increasing the destruction rate of the doubly excited states. Thus collisions effectively increase the branching ratio for dielectronic capture. As the electron density becomes high enough this effect will also saturate as the branching ratio reaches unity. It should be pointed out, of course, that at these high values of n_e collisional excitation from the sodium-like

non-autoionizing states(which do have a finite population) will cause a reverse flow and counterbalance the dielectronic recombination.

Finally, the dielectronic rate coefficient we have calculated is only a partial rate coefficient. Accurate calculations of the rate coefficient must include principal quantum numbers up to a limit dictated by plasma ionization. We are currently calculating the contributions of the nln'l' manifolds for $n,n' \geq 3$. Convergence of the calculated rates is expected to be fairly rapid for high Z ions, such as tungsten, for two reasons. First, calculations using the 3l3l' manifold for tungsten show that the bulk of the dielectronic recombination flux proceeds through a reasonably small number of channels. Secondly, due to jj coupling, each multiconfiguration wave function used to calculate matrix elements is very pure in one single configuration wavefunction for the high Z ions. In this case, the use of single configuration wavefunctions should be a very good approximation and extension of the dielectronic rate coefficient to high n values can be accomplished quite accurately by semianalytic formulation. Convergence of the low Z cases, on the other hand, is complicated by the necessity of including virtually all of the 3l3l' states to obtain reasonable accuracy.(The results reported here include all states for each calculation.) However, including principal quantum numbers above n=4 will require compromise due to the large number of states for these manifolds. Despite a lower plasma ionization principal quantum number for low Z ions, computation of converged dielectronic rate coefficients for these elements becomes very difficult because of the necessity of retaining virtually every state of the doubly excited manifolds.

The authors would like to thank Rosemary Jung for her invaluable assistance in organizing the computer coding which makes up YODA. The authors would also like to thank L. R. Roszman and S. M. Younger for many useful suggestions.

References

1. A. Burgess, Astrophys. J. 139, 776 (1964).

2. A. L. Merts, R. D. Cowan, and N. H. Magee, Jr., Los Alamos Scientific Laboratory Report No. LA-6220-MS, 1976(unpublished).

3. Y. Hahn, J. N. Gau, R. Luddy, and J. A. Retter, J. Quant. Spectrosc. Radiat. Transfer 23, 65 (1980).

4. Larry J. Roszman, Phys. Rev. A 20, 673 (1979).

5. B. W. Shore, Astrophys. J. 158, 1205 (1969).

6. A. Burgess and H. P. Summers, Astrophys. J. 157, 1007 (1969).

7. P. J. Mohr, Ann. Phys. 88, 26 (1974).

8. E. A. Uehling, Phys. Rev. 48, 55 (1935).

9. A. Burgess, J. Phys. B 7, L364 (1974).

10. M. J. Seaton and P. J. Storey, "Atomic Processes and Applications", N. Holland (1976).

11. A. Burgess, Astrophys. J. 141, 1588 (1965).

12. J. C. Weisheit, J. Phys. B 8, 2556 (1975).

Table I			
Z	θ_0(in eV)	α_{MAX}^{DR} ($10^{-11} cm^3/sec$)	$\bar{E}$(in eV)
18	124	.265	186.5
26	257	.825	385.6
29	314	1.109	471.6
32	380	1.235	569.8
36	474	1.382	711.0
40	576	1.489	864.3
41	602	1.495	903.4
42	632	1.488	948.4
44	692	1.470	1037.8
45	724	1.451	1085.3
47	788	1.441	1181.4
50	885	1.423	1326.9
54	1023	1.389	1533.6
60	1257	1.178	1881.4
67	1556	1.009	2327.5
73	1844	.865	2752.4
74	1881	.845	2806.5

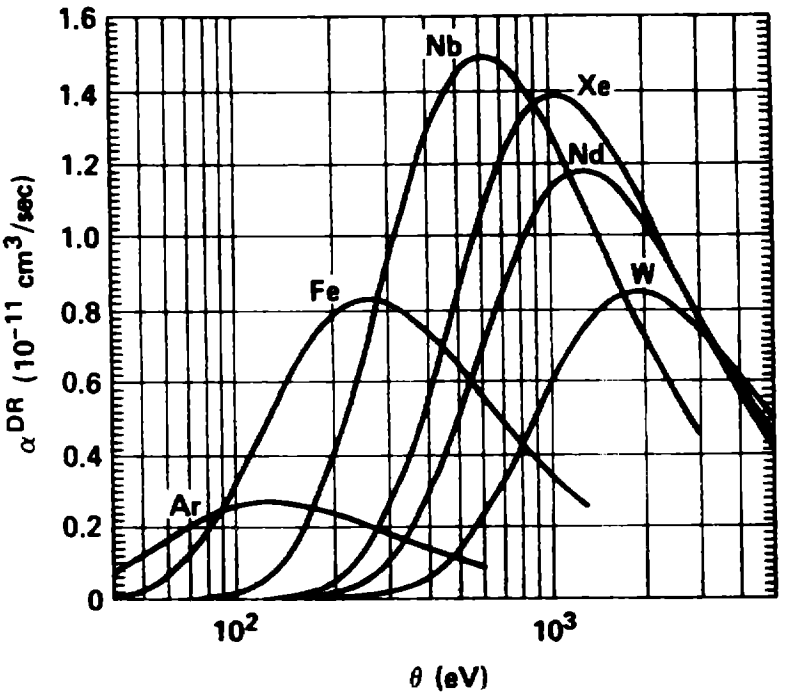

Figure 1 Dielectronic rate coefficient α^{DR} versus electron temperature for six neon-like ions.

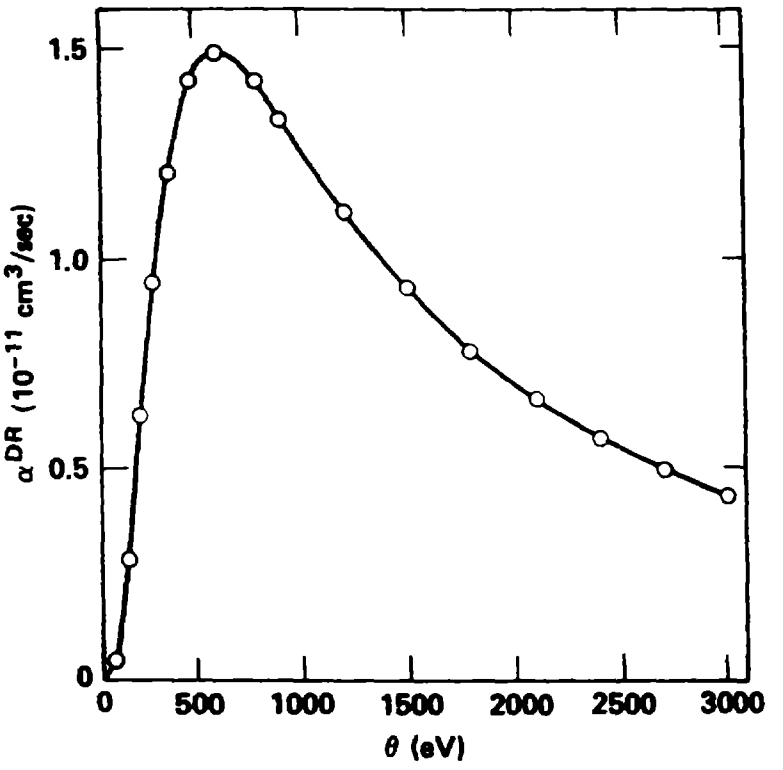

Figure 2 Dielectronic rate coefficient α^{DR} versus electron temperature for neon-like niobium. The circles are the result of this calculation while the solid line is the theoretical fit of equation 15.

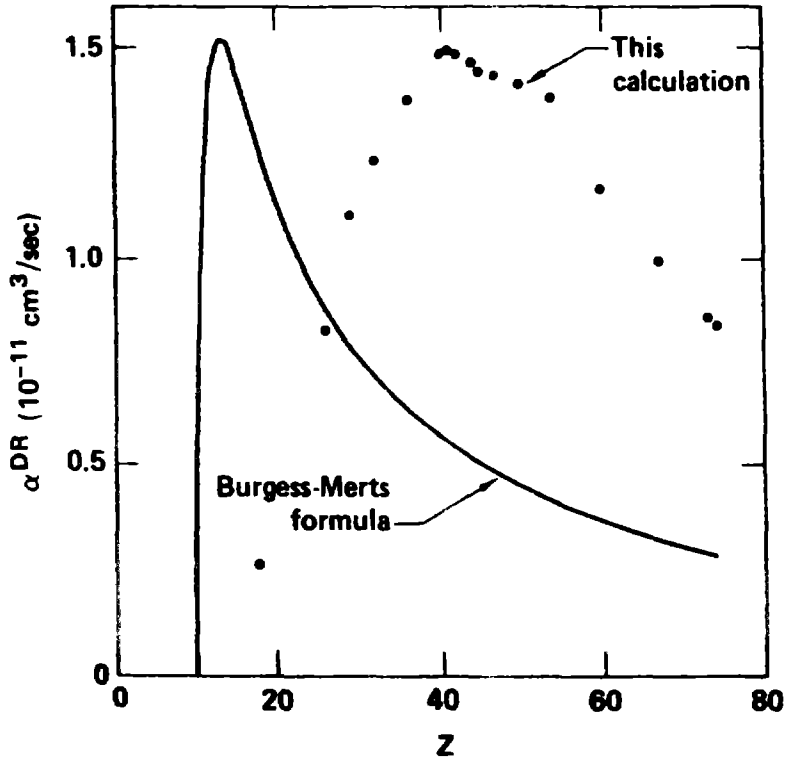

Figure 3 The maximum value of the dielectronic rate coefficient α^{DR} versus the bare nuclear charge Z for seventeen neon-like ions. The open circles are a result of this calculation while the solid line is calculated from the Burgess-Merts formula.

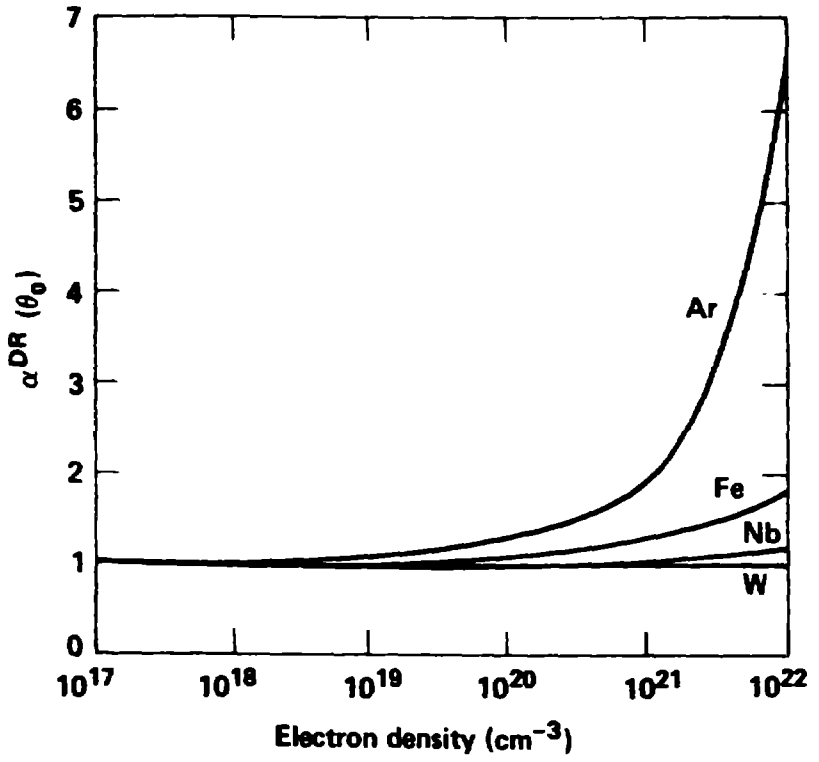

Figure 4 Dielectronic rate coefficient $\alpha^{DR}(\theta_0)$ versus electron density for several neon-like ions. The curves are normalized to unity at $n_e = 10^{14}$.

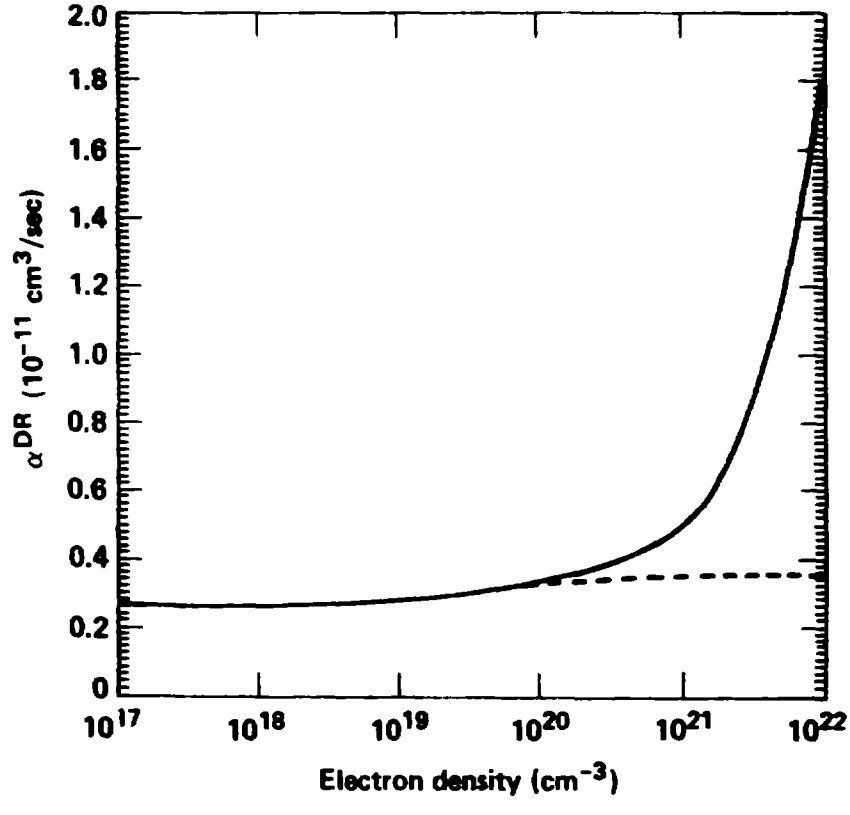

Figure 5 Dielectronic rate coefficient $\alpha^{DR}(\theta_0)$ versus electron density with(solid line) and without(dashed line) electron collisional de-excitation($\Delta n = 1$) for neon-like argon.